International Journal of Modern Physics: Advances in Theory and Application
Vol. 2, Issue 1, 2017, Pages 149-182
Published Online on February 1, 2017

http://jyotiacademicpress.org

THERMAL ANNEALING AND SUBSTRATE NATURE EFFECTS ON STRUCTURAL PROPERTIES, MORPHOLOGICAL AND PHOTOLUMINESCENCE OF PLANAR $Y_2O_3 : Eu^{3+}$ THIN FILM PHOSPHORS DEPOSED BY SOL-GEL METHOD

L. GUERBOUS[1], A. BOUKERIKA[1], M. TAIBECHE[1], A. SARI[2], Y. LARBAH[1], M. SERAICHE[1], M. S. E. HAMROUN[1], S. SAADI[1], L. LAMIRI[3] and B. KAHOUADJI[3]

[1]Laser Department
Nuclear Research Center of Algiers-CRNA
02 Bd. Frantz Fanon
BP 399 Algiers
Algeria
e-mail: guerbous@yahoo.fr

[2]Nuclear Research Center of Birine, 'CRNB'
P.O. Box 180
17200 Aïn-Oussera, Djelfa
Algeria

[3]Faculté des Sciences Exacts
Département de Physique
Université de Béjaia, 06000
Algeria

Keywords and phrases: $Y_2O_3 : Eu^{3+}$, thin film, nano-phosphor, spin-coating, photoluminescence.

Communicated by Mesfin Kebede.
Received December 24, 2016; Revised January 13, 2017

Abstract

Intense red emission extracted from $Y_2O_3:Eu^{3+}$ planar phosphor thin films have been successfully grown on different substrates such as Si (100), Si (111), and corning glass using spin-coating derived sol-gel deposition technique. The thin films are annealed at different temperatures. X-ray diffraction (XRD), FE-SEM, FTIR as well as steady and time resolved photoluminescence (PL) techniques were used to characterize the $Y_2O_3:Eu^{3+}$ phosphor films. The cubic phase of Y_2O_3 is identified and it is found that the nano-particles sizes increase when increasing annealing temperature for Si (100), Si (111) substrates. Under UV excitation, the $Y_2O_3:Eu^{3+}$ films show strong red emission at the 611nm assigned to forced electric dipole transition $^5D_0 \rightarrow {}^7F_2$ of Eu^{3+} in C_2 cite. The emission spectra also show the other intra-configurational transitions $^5D_0 \rightarrow {}^7F_J$ ($J = 0, 1$). The PL excitation spectra show only the charge transfer energy from the O^{2-} to Eu^{3+}. A blue-shift of the charge-transfer (CT) band in excitation spectra was observed in $Y_2O_3:Eu^{3+}$ thin films compared with bulk $Y_2O_3:Eu^{3+}$. Room temperature time-resolved emission spectra were measured; the variation of $^5D_0 \rightarrow {}^7F_2$ emission, decay time and refractive index with substrate nature and annealing temperature are discussed.

1. Introduction

The excellent thermal stability and light output of RE (rare earth) phosphorus doped oxide have given more importance to the application related scintillation materials and display devices such as CRT (cathode ray tube), LED (light emitting diode), and fluorescence lamp [1-5]. Indeed, required by the increasing demand of the X ray thin film inorganic scintillator detectors for X-CT application, flat panel display and similar field emission display devices, preparation and characterization of thin film phosphors have been an important research topic. Compared with powder phosphor, thin film phosphors have advantages of better thermal stability, better adhesion to substrates, better uniformity and higher resolution. It is known that yttrium oxide

(Y_2O_3) is an excellent host material for rare earth ions doping and presents as a potential host for integrated optics because of the good qualities, such as broad transparency range (0.2-8μm), high refractive index (> 1.9), large band gap (5.8eV), excellent physical and chemical stability, low phonon energy, and high dielectric constant (ε = 14-18) [6]. Furthermore, for thin films it present low lattice mismatch with Si ($a_{Y_2O_3} = 1.060\text{nm}$, $a_{Si\times2} = 1.086\text{nm}$) as substrate. This is the reason that $Y_2O_3 : Eu^{3+}$ phosphor is one of the best red phosphors used for more than 40 years since 1964 [7]. $Y_2O_3 : Eu^{3+}$ thin film phosphor can be synthesized by several different methods such as pulsed laser deposition (PLD) [8], atomic layer deposition (ALD) [9], chemical vapor deposition (CVD) [10], sputtering [11], spray-pyrolysis [12] , electrospray [13], and spin-coating technique [14]. The last technique is relatively easy and economical to prepare uniform nanosized, high quality stoichiometric thin film phosphors and at low temperatures. It is still a challenge the improvement of structural and photoluminescence properties of $Y_2O_3 : Eu^{3+}$ thin films to build optical devices with high performance. In addition, for phosphor thin-film applications the extraction efficiency and the internal quantum efficiency of such are both important factors in the external efficiency [15]. It should be noted that the luminescence efficiency of thin film phosphor has never exceeded that of powder. This is due to the poor light extraction efficiency of thin-film phosphors, resulting from the high refractive index, leading the light guiding effect. In fact, only a small fraction of the total number of emitted photons generated inside phosphor films can escape because of the total internal reflection due to its high refractive index. Therefore, increasing the light extraction efficiency from the phosphor films is a critical issue for advanced thin film phosphor in several applications.

In this work, intense red powders and planar $Y_2O_3 : 5\% Eu^{3+}$ thin film phosphors, deposited on different type substrates Si (100), Si (111), and corning glass, annealed at different temperatures were synthesized by sol-gel spin-coating technique. A systematic study of structural,

morphological, room temperature steady and time-resolved luminescence properties is reported. This work aims also to investigate the influence of substrate nature and annealing temperature on the light extraction from $Y_2O_3 : 5\% Eu^{3+}$ thin film phosphors.

2. Experimental

2.1. Synthesis

The $Y_2O_3 : 5\% Eu^{3+}$ phosphor powders and thin films were prepared by the sol-gel process. High purity yttrium oxide Y_2O_3, 99.999% and europium oxide (Eu_2O_3, 99.999%) were used as starting materials. Stoichiometric amounts of each oxide were dissolved in dilute nitric acid (HNO_3) and the mixed solution was stirred at room temperature for 24h to get transparent precursor solution. The pH of the solution was adjusted to 5 by adding ammonium hydroxide (NH_3OH). As for the $Y_2O_3 : Eu^{3+}$ mentioned below in the comparative experiments, the doping level of Eu^{3+} ion is 5% (nominal composition). For obtaining the $Y_2O_3 : Eu^{3+}$ nanopowders, the resulting solution were dried at 120°C until transforming into a black bulk. Finally, the powders (black bulk) were introduced in a special furnace and heated in air at various temperatures: 500ºC, 650ºC, 800ºC, and 950ºC for 2 hours. For $Y_2O_3 : Eu^{3+}$ thin films deposited on Si (100), Si (111), and corning glass 7059 substrates, the mixed solutions were spun with a speed of 3000rpm for 30s after the sol deposition. To make a constant thickness, for each substrate, the operation is repeated 12 times and dried in air at 150ºC. In the end, the films samples deposited on Si (100) and Si (111) are annealed at 500ºC, 650ºC, 800ºC and 950ºC, while those on corning glass 7059 are annealed at 500ºC and 650ºC for 2 hours duration. Figure 1 shows schematic process used to prepare the $Y_2O_3 : 5\% Eu^{3+}$ powders and thin-film phosphors.

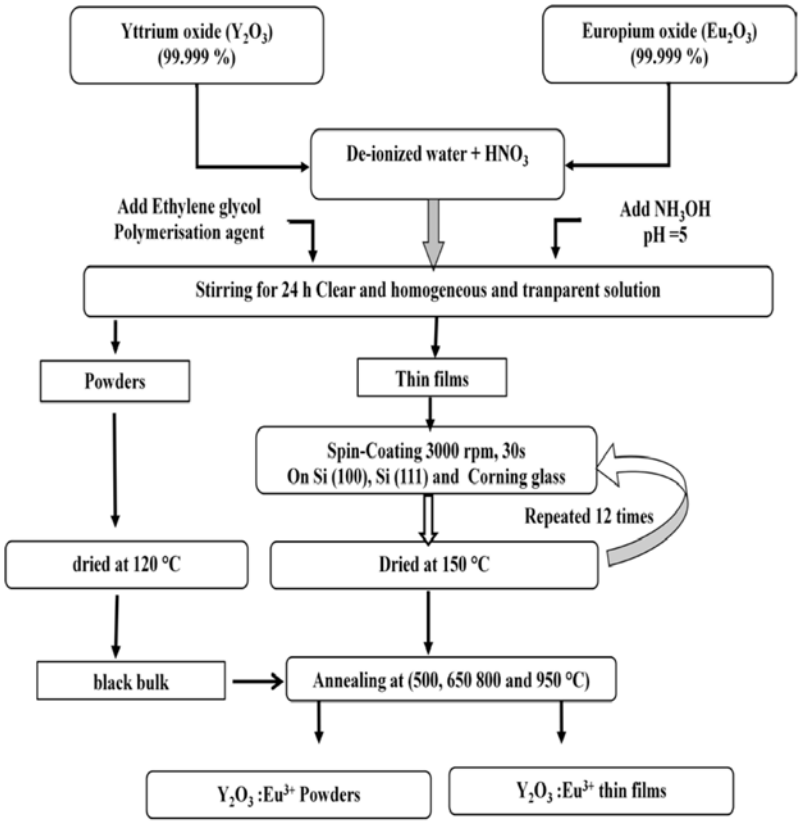

Figure 1. Scheme for the preparation of the $Y_2O_3 : Eu^{3+}$ powder and thin-film nanophosphors by sol-gel spin-coating.

2.2. Characterization

The crystalline structure of the $Y_2O_3 : Eu^{3+}$ thin films was investigated by the X-ray diffraction (XRD) technique using a Philips X'Pert Pro diffractometer using CuK_α radiation ($\lambda = 1.54059 Å$) operated at 40kV and 30mA in grazing incidence mode. The morphology of thin films have been carried out by using a Philips XL 30 field emission scanning electron microscope. The steady and time-resolved photoluminescence spectra were carried out using Perkin-Elmer (LS-50B) luminescence spectrometer with pulsed Xe lamp excitation at room temperature as described in [16].

3. Results and Discussion

3.1. XRD and structure of the thin films

Figure 2 ((a), (b), (c) and (d)) shows the XRD profiles of Y_2O_3 : 5% Eu^{3+} powders (Figure 2(a)) and thin films deposited on Si (100) (Figure 2(b)), Si (111) (Figure 2(c)), and corning glass 7059 (Figure 2(d)), annealed at different temperature. All XRD patterns are compared to that of as-prepared samples and to JCPDS Card 25-1200 for Y_2O_3. All diffraction peaks are attributed to the pure body-centered cubic (bcc) structure for Y_2O_3 phase and match well with JCPDS (25-1200) card with space group Ia3. For all as-prepared powders and thin films, no characteristic peak corresponding to Y_2O_3 was observed. For powders (Figure 2(a)) shows five main peaks are observed, which can be assigned to (211), (222), (400), (440), (622) of cubic Y_2O_3. Furthermore, the peaks become much more intense and sharper with increasing temperature, which indicates that the crystallinity become well better and the crystallite size increased. As seen from Figure 2(b), firing at 500°C, all powders and thin films samples present reflection at around 29°, assigned to (222) of cubic Y_2O_3, indicating the starting of crystallization. For Si (100) and Si (111) substrates, the peak (222) is more intense than of corning glass, which presents a broad and weak peak. Furthermore, on Si (111), at this annealing temperature (500°C) an additional resolved peak located at around 48°, corresponding to (440) peak reflection is observed. With the increase of the annealing temperature (222) peak become stronger due to the increase of crystallinity, and other diffraction peaks at (400), (440), and (622) belonging to the crystalline Y_2O_3 can be observed and which are in good agreement with those of the JCPDS Card 25-1200. For corning glass substrate, in addition to (222) peak, only a broad peak correspond to (440) peak is observed at 650°C. The average crystallite size 'D' of Y_2O_3 : Eu^{3+} powders can be estimated by using the Scherrer's

formula [17]: $D_{Sch} = \frac{0.9 \times \lambda}{\beta_{sample} \cos\theta}$, where $\lambda = 1.54059\text{Å}$ is the wavelength of the X-ray radiation used, where D_{Sch} is the crystallites size in nm, λ is the diffractometer wavelength in nm, $\beta_{sample} = \sqrt{\beta_{\exp}^2 - \beta_{ins}^2}$, $\beta_{\exp}$ is the full width at half maximum in the (222) reflection, β_{ins} is the correction factor for instrument broadening, and θ is the diffraction angle. The lattice parameters a can be calculated by using the following formula: $a^2 = \frac{\lambda^2 \times (h^2 + k^2 + l^2)}{4 \sin^2\theta}$, where a is the lattice parameter and (hkl) is the Miller index of the crystal plane. The average crystallite size and crystallographic unit cell parameters were calculated and listed in Table 1. From Table 1, we see that the crystallite size of synthesized $Y_2O_3 : 5\% Eu^{3+}$ powders and thin films increased with increasing annealing temperature. It is found that the crystallite size of powders is always bigger than that in thin films whatever the substrate and the annealing temperature. On corning glass substrate the crystallite size remains the same for 500°C and 650°C annealing temperatures. We note also that on Si (111) substrate $Y_2O_3 : 5\% Eu^{3+}$ exhibit smaller grain size than on Si (100). The lattice parameter varies randomly with temperature and substrate nature compared to the reported value for bulk Y_2O_3 is 10.604Å (JCPDS 25-1200).

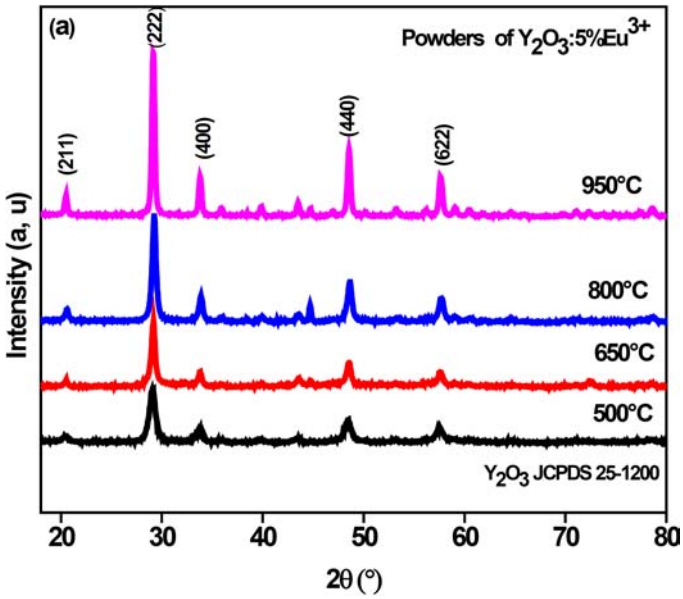
(a)
Powders of Y_2O_3:5%Eu^{3+}
(222)
(211)
(400)
(440)
(622)
950°C
800°C
650°C
500°C
Y_2O_3 JCPDS 25-1200
Intensity (a, u)
20
30
40
50
60
70
80
2θ (°)

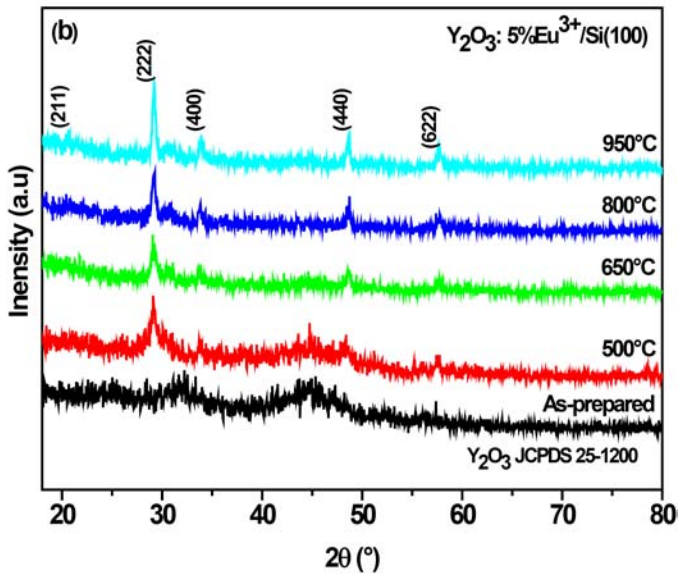
(b)
Y_2O_3: 5%Eu^{3+}/Si(100)
(211)
(222)
(400)
(440)
(622)
950°C
800°C
650°C
500°C
As-prepared
Y_2O_3 JCPDS 25-1200
Inensity (a.u)
20
30
40
50
60
70
80
2θ (°)

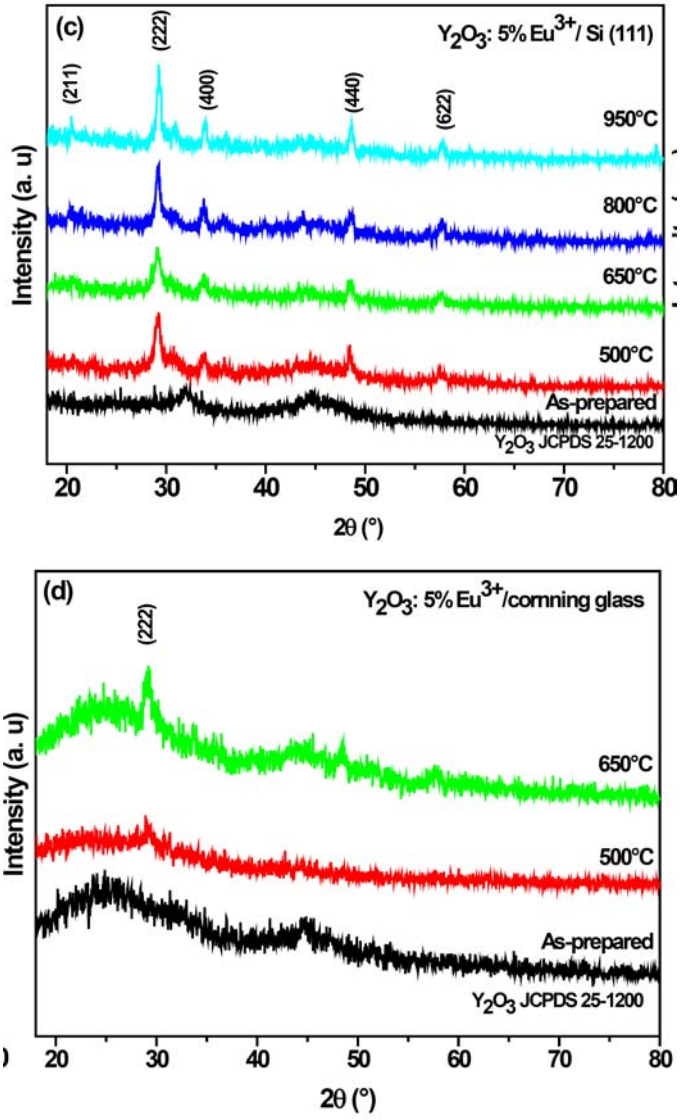

Figure 2. Comparison of XRD patterns for the Y_2O_3 : 5% Eu^{3+} powder (a) and thin films, deposited on (b) Si (100), (c) Si (111), and (d) glass corning substrates, annealed at different temperatures.

Table 1. Structural parameters of Y_2O_3 : 5 at % Eu^3 powders and thin films samples on different substrate and at different annealing temperatures

T(°C)	Powder		Si (100)		Si (111)		Corning glass	
	a(Å)	D(nm)	a(Å)	D(nm)	a(Å)	D(nm)	a(Å)	D(nm)
500	10.655	12	10.648	4	10.583	9	10.847	6
650	10.628	20	10.588	12	10.621	8	10.584	6
800	10.608	30	10.811	19	10.580	11		
950	10.612	40	10.599	24	10.506	16		

3.2. Morphology of $Y_2O_3 : Eu^{3+}$ thin films

It is well knowing that the surface morphology of $Y_2O_3 : Eu^{3+}$ thin-film materials have an important effect on the photoluminescence response. Furthermore, the annealing temperature and the nature of substrates are critical parameters for preparation of well-crystallized, smooth-surface thin film. FE-SEM micrographs revealed different morphology features of Y_2O_3 : 5% Eu^{3+} films at different temperatures, as shown on Figure 3 (a)-(f). Films deposited on Si (100), annealed at 500°C (Figure 3(a)) and presents a surface with smooth and covered with granular morphology and is cracks free. When annealing temperature increases at 950°C (Figure 3(b)), the film surface become dense, very smooth and also cracks free, which in good agreement with XRD analysis. For films on Si (111) substrate, annealed at 500°C (Figure 3(c)), present also granular morphology and some cracks, pores, likely due to material loss during annealing. Annealing at 950°C (Figure 3(d)), present films with granular morphology, free of cracks and the pores remain exist. For films deposited on amorphous glass corning substrate, at 500°C (Figure 3(e)), it shows particles closely packed, well-distributed and exhibiting a homogeneous surface morphology. Increasing the annealing temperature at 650°C (Figure 3(f)), the surface become more homogeneous and present some cracks and free of pores. According to Cho et al. [15], the occurrence

of cracks in the $Y_2O_3 : Eu^{3+}$ phosphor thin films can be mainly due to the difference between the thermal expansion coefficients of Y_2O_3 and the substrate materials. In general, the FE-SEM images confirm that crystalline and smooth $Y_2O_3 : Eu^{3+}$ thin-film phosphors are obtained through the sol-gel spin coating and annealing processes.

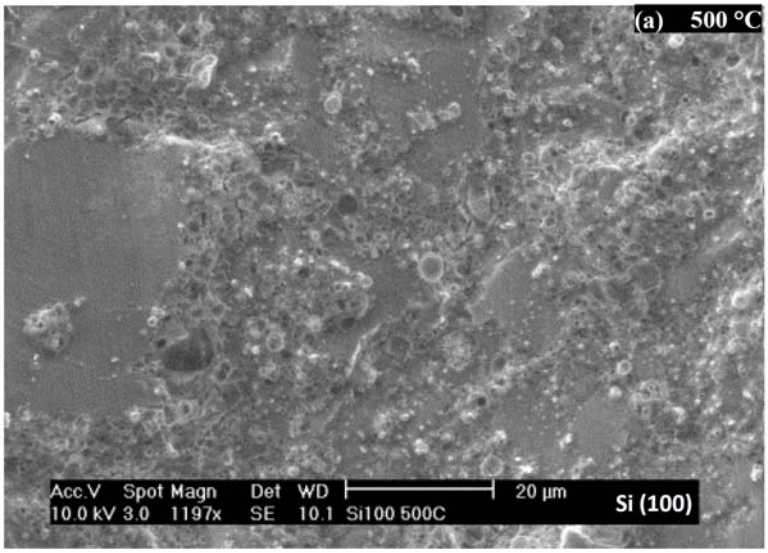
(a) 500 °C
Acc.V Spot Magn Det WD 20 µm
10.0 kV 3.0 1197x SE 10.1 Si100 500C
Si (100)

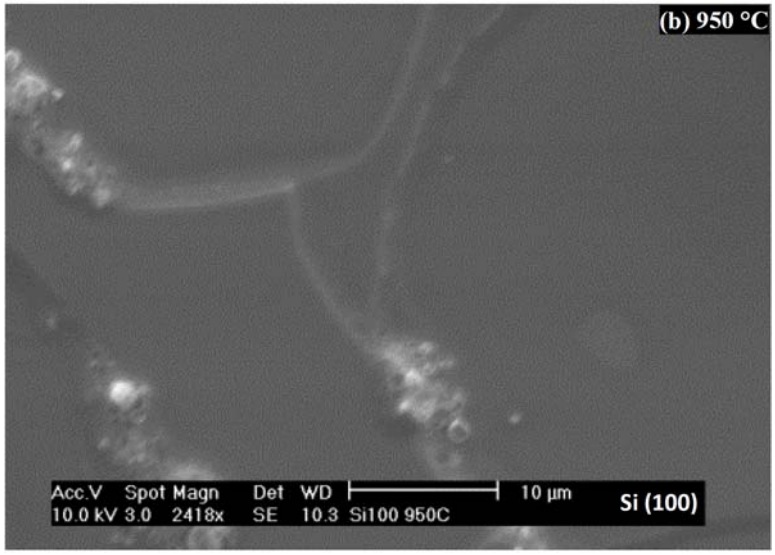
(b) 950 °C
Acc.V Spot Magn Det WD 10 µm
10.0 kV 3.0 2418x SE 10.3 Si100 950C
Si (100)

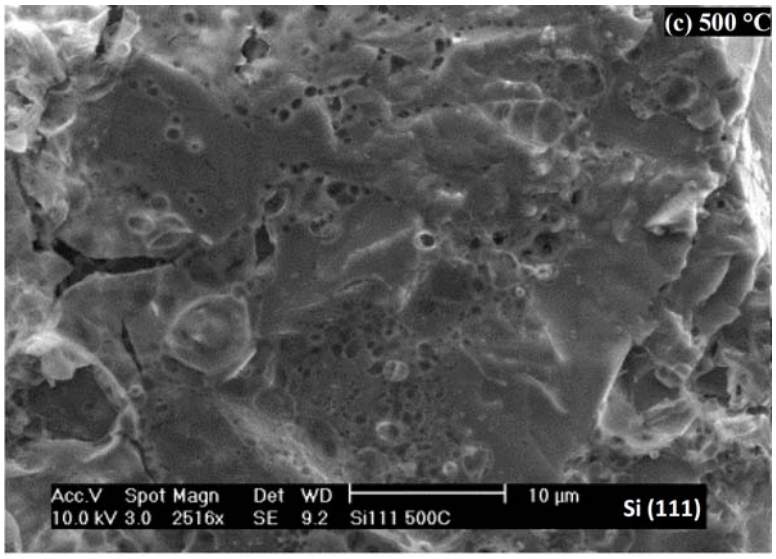
(c) 500 °C
Acc.V Spot Magn Det WD 10 µm
10.0 kV 3.0 2516x SE 9.2 Si111 500C
Si (111)

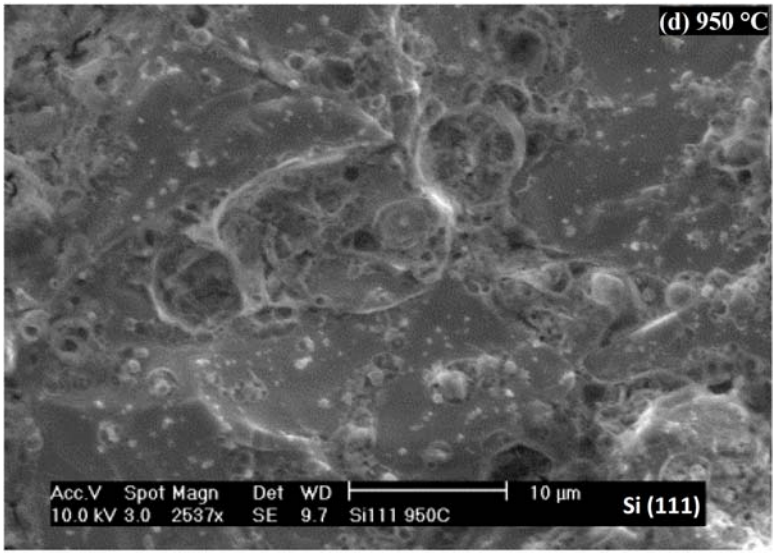
(d) 950 °C
Acc.V Spot Magn Det WD 10 µm
10.0 kV 3.0 2537x SE 9.7 Si111 950C
Si (111)

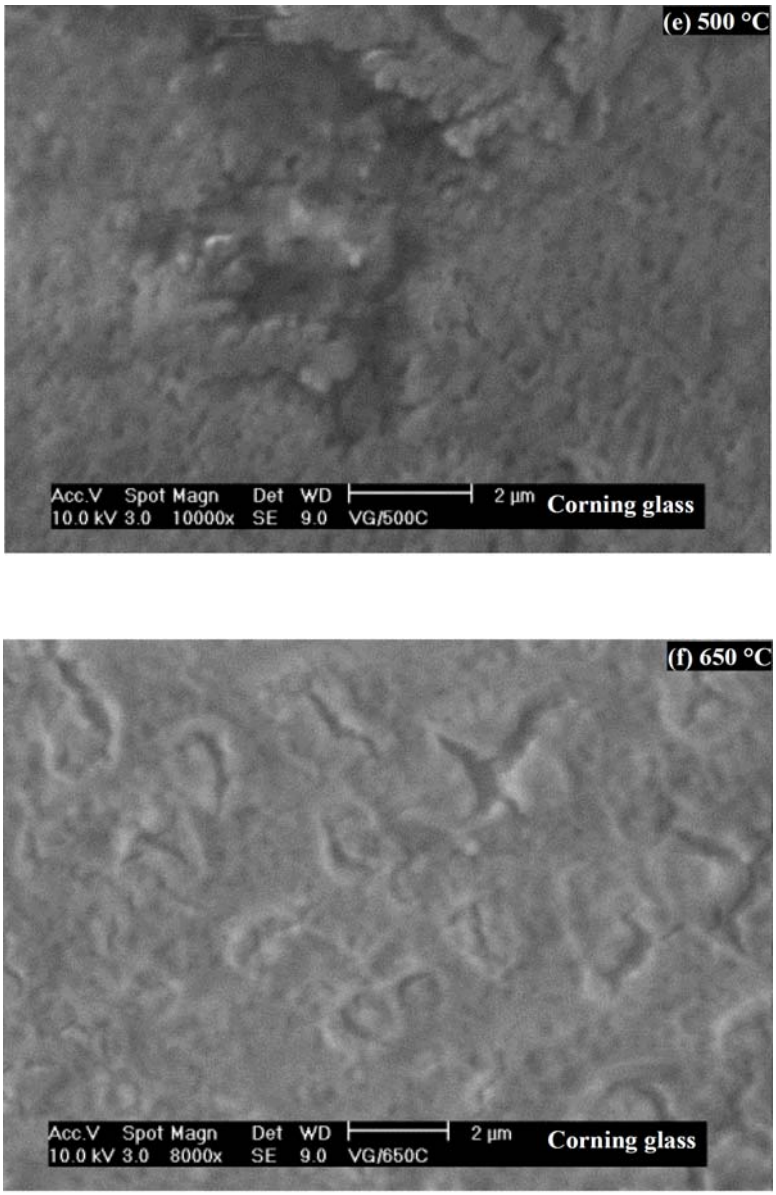

Figure 3. FE-SEM images of the Y_2O_3 : 5% Eu^{3+} thin films, (a), (b) Si (100) for 500°C and 950°C, (c), (d) Si (111) for 500°C and 950°C, (e), (f) corning glass for 500°C and 650°C.

3.3. Steady photoluminescence spectroscopy

On Figure 4(a)-(d), we display respectively, the room temperature steady emission spectra of Y_2O_3 : 5 at. % Eu^{3+} powders and thin films, deposited on Si (100), Si (111) and glass corning substrates, annealed at different temperature. These spectra are measured between 500nm and 700nm, excited at 230nm, corresponding to the charge transfer band (CTB). The electric dipole transition $^5D_0 \rightarrow {}^7F_2$ lines displaying peaks at 611nm, very characteristic to typical of the cubic phase Y_2O_3 and is sensitive to the local environment of the Eu^{3+} ions. This transition dominates in intensity relative to the magnetic dipole $^5D_0 \rightarrow {}^7F_1$ transition, indicating that Eu^{3+} occupies a crystallographic site with no inversion symmetry (C_2) [16, 19]. The weak peak centered at 630nm is assigned also to $^5D_0 \rightarrow {}^7F_2$ transition. Also, peaks centered at 588nm, 595nm, and 598nm are due to the forced magnetic dipole $^5D_0 \rightarrow {}^7F_1$ transition. The peak observed at 580nm, is attributed to the $^5D_0 \rightarrow {}^7F_0$ transition. The comparison of emission intensities at wavelength 611nm (corresponding to $^5D_0 \rightarrow {}^7F_2$ transition) and the asymmetric ratio of luminescence (defined as A_{21}) for different annealing temperatures are shown in Figure 4 ((a)-(d) insets). In fact, the asymmetric ratio of luminescence (defined as A_{21}) of Eu^{3+} ions is sensitive to the environment around the Eu^{3+} ion as well its concentration. It is defined as the ratio of intensity of the electric dipole transition ($^5D_0 \rightarrow {}^7F_2$ at 611nm) to that of the magnetic dipole transition ($^5D_0 \rightarrow {}^7F_1$ at 595nm): $A_{21} = I(^5D_0 \rightarrow {}^7F_2) / I(^5D_0 \rightarrow {}^7F_1)$ [19]. For Y_2O_3 : 5% Eu^{3+} powders samples, it is observed that the PL intensity at 611nm increases with increasing the annealing temperature and A_{21} follows the same behaviour and present a high values. As it is know that in the cubic

Y_2O_3 lattice Eu^{3+} ion can occupy two different types of crystallographic positions: one is the 24d site with C_2 symmetry and the other is the 8b site with S_6 inversion symmetry. Furthermore, the ratio of C_2 to S_6 is 3 : 1 (75% and 25% of the total Y^{3+} ions occupied the C_2 and S_6 sites, respectively), then the Eu^{3+} ions are expected to occupy these two sites in a statistical point of view replacing Y^{3+} ions. As it is known that $^5D_0 \rightarrow {}^7F_2$ transition (611nm) arose from the C_2 site while $^5D_0 \rightarrow {}^7F_1$ (595nm) emission arose from the S_6 site for Eu^{3+}, the much higher occupancy of the C_2 sites results in an increased A_{21} ratio, along with cation homogenization.

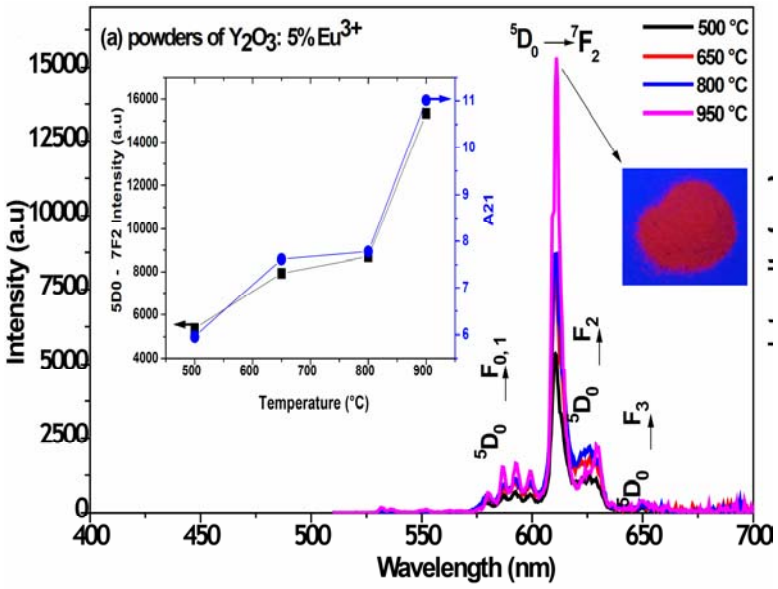
(a) powders of Y_2O_3: 5% Eu^{3+}
$^5D_0 \rightarrow {}^7F_2$
500 °C
650 °C
800 °C
950 °C
Intensity (a.u)
Wavelength (nm)
5D0 - 7F2 Intensity (a.u)
A21
Temperature (°C)
$^5D_0 \rightarrow F_{0,1}$
$^5D_0 \rightarrow F_2$
$^5D_0 \rightarrow F_3$

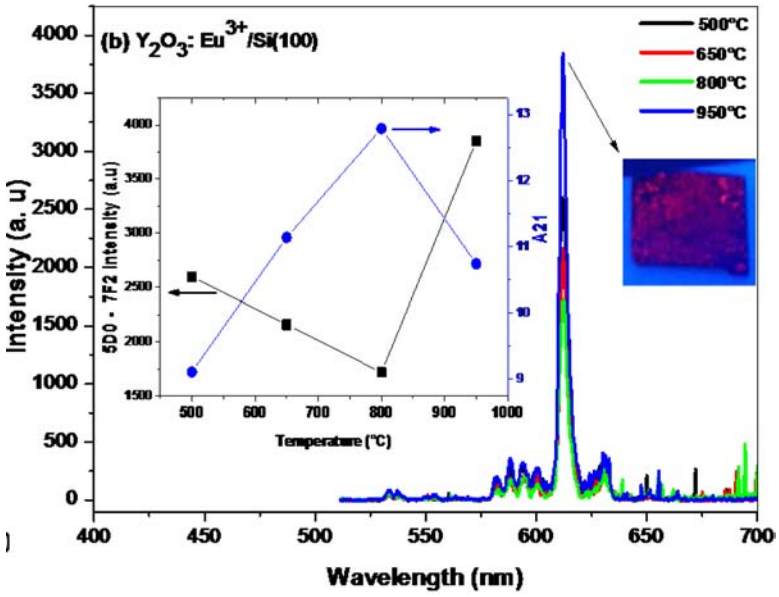
(b) Y_2O_3: Eu^{3+}/Si(100)
500°C
650°C
800°C
950°C
Intensity (a. u)
Wavelength (nm)
5D0 - 7F2 Intensity (a.u)
A21
Temperature (°C)

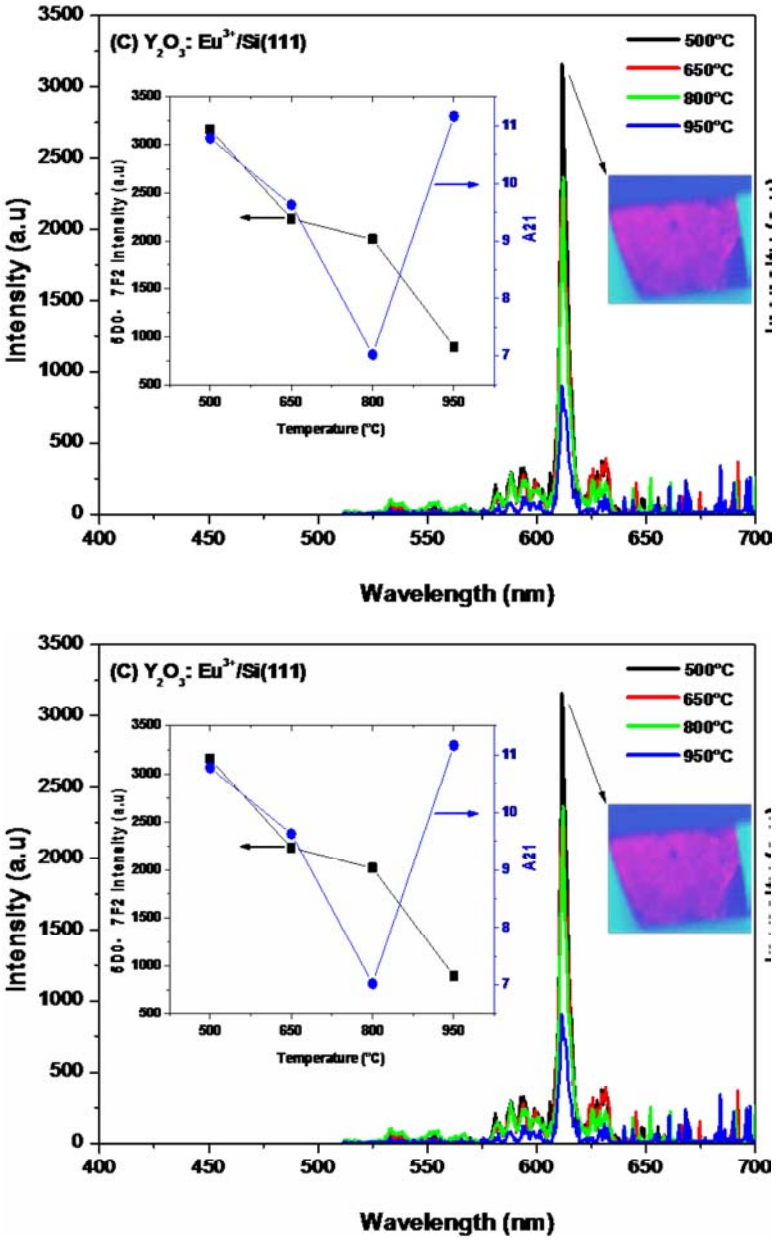

Figure 4. Room temperature steady emission spectra of Y_2O_3 : 5% Eu^{3+} powder (a) and thin films, deposited on (b) Si (100), (c) Si (111), and (d) glass corning substrates, annealed at different temperatures.

For $Y_2O_3 : Eu^{3+}/Si$ (100), despite the decreasing of $^5D_0 \rightarrow {}^7F_2$ intensity from 500°C to 800°C with the annealing temperature, A_{21} increases and decrease when $^5D_0 \rightarrow {}^7F_2$ intensity decreases from 800°C to 950°C. In the other side, for $Y_2O_3 : Eu^{3+}/Si\,(111)$, $^5D_0 \rightarrow {}^7F_2$ intensity decreases from 500°C to 800°C and A_{21} follows the same behaviour, but from 800°C to 950°C, it increases counterclockwise $^5D_0 \rightarrow {}^7F_2$ intensity which increases. For the corning glass substrate, from 500°C to 650°C, A_{21} present the same behaviour and increases as $^5D_0 \rightarrow {}^7F_2$ intensity. It is important to note that on all substrates and annealing temperature, the $^5D_0 \rightarrow {}^7F_2$ intensity decreases despite that A_{21} present a highly values, which indicate that the local environment of the Eu^{3+} ion is notably distorted, in agreement with a C_2 symmetry for the sites mainly occupied by the dopant ions.

In Figure 5, we displays the evolution of the ratio of $^5D_0 \rightarrow {}^7F_2$ emission transitions intensities of the thin films to the same transition in powders $(R = I(^5D_0 \rightarrow {}^7F_2)_{\text{thin film}} / I(^5D_0 \rightarrow {}^7F_2)_{\text{powder}})$. One can assume that this ratio represent the percentage of light extracted from the thin films. As seen from the figure, for Si (100) and Si (111) substrates, this ratio decreases with increasing the annealing temperature. At 500°C, the ratio can reach 60% for Si (111) and 50% for Si (100). For the corning, it increases from 15% at 500°C to 45% at 650°C. Despite that at 500°C Y_2O_3 doped Eu^{3+} nanomaterial present the very small grain size relative to the other temperature, it exhibit the strong light extraction from the thin film.

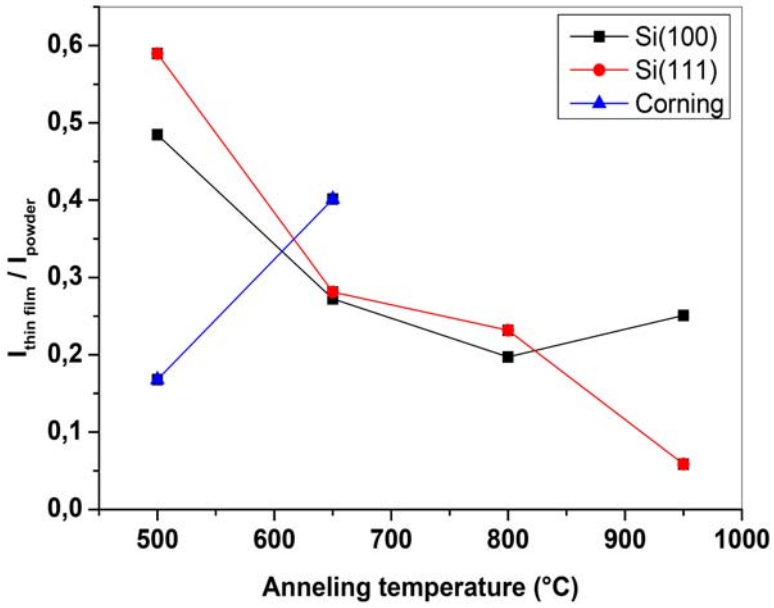

Figure 5. The evolution of $I(^5D_0 \rightarrow ^7F_2)_{thin\ film}/I(^5D_0 \rightarrow ^7F_2)$ ratio for different type of substrate and temperature.

This anomalous behaviour of the $Y_2O_3 : Eu^{3+}$ thin film emission intensity, the asymmetric ratio as well as the light extraction depends definitely on the substrate nature and the annealing temperature, but, they depends by other factors generated by the crystallographic parameters. Figure 6 displays the excitation spectra of $Y_2O_3 : 5\%\ Eu^{3+}$ thin films deposited on Si (100), Si (111) annealed at 950°C and corning glass at 650°C, corresponding to two different $Y_2O_3 : Eu^{3+}$ grain size. These spectra are obtained by monitoring the red emission wavelength fixed at 611nm, that corresponding to $^5D_0 \rightarrow ^7F_2$ transition between 200 and 300nm. All spectra exhibit a first broad band between 200-220nm, assigned to the host absorption of Y_2O_3, i.e., transition from 2p orbital of O^{2-} (valence band) to 5d-6s orbitals of Y^{3+} (conduction band). The second one is abroad and strong band, localized between 220-280nm

attributed to $O^{2-} \rightarrow Eu^{3+}$ charge transfer band (CTB), i.e., the electron transfer from the 2p orbital of O^{2-} (valence band) to the empty 4f orbital of Eu^{3+} ion, leading to Eu^{2+} ion in his ground state. This CT band shift to the short wavelengths region (blue shift) with increasing the annealing temperatures or grain size. The same phenomenon has been observed in $Y_2O_3 : Eu^{3+}$ nano powders in our previous work [16] and to explain this shift, a modified Jørgensen expression is proposed based on Eu^{3+}-O^{2-} distance and the coordination number variations.

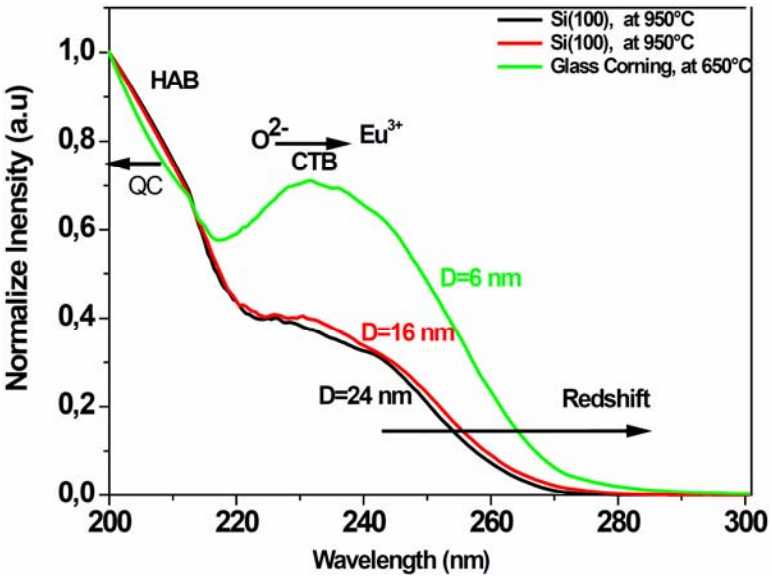

Figure 6. Room temperature excitation spectra of $Y_2O_3 : 5\% Eu^{3+}$ thin films deposited on Si (100), Si (111) annealed at 950°C and corning glass at 650°C.

Figure 7 exhibit CIE 1931 *x y* chromaticity diagram is also plotted for further analysis of the thin film phosphors. It is clear from that the thin films on Si (100) and Si (111) are closed to the $Y_2O_3 : Eu^{3+}$ red phosphor, but for corning it present a pronounced deviation, assigned to the nature substrate.

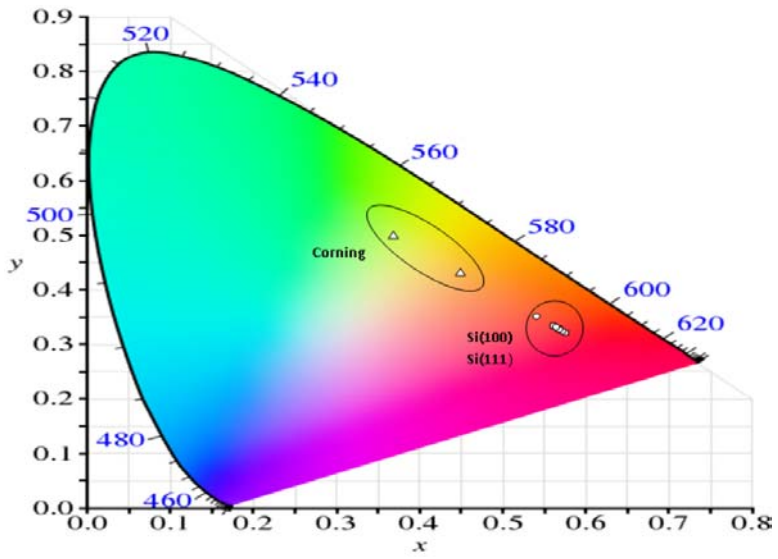

Figure 7. CIE chromaticity diagram showing the *x*, *y* emission color coordinates for the $Y_2O_3 : 5\% Eu^{3+}$ thin films nanophosphors for different substrate and annealing temperature.

3.4. Time-resolved photoluminescence spectroscopy

The room temperature time-resolved emission spectra of $Y_2O_3 : 5\% Eu^{3+}$ Eu^{3+} thin films, deposited on Si (100), Si (111), and glass corning substrates, annealed at different temperature are displayed on Figure 8 ((a), (b) and (c)) are measured. The photoluminescence decay curves of the $^5D_0 \rightarrow {}^7F_2$ transition (611nm) of Eu^{3+} ions in the Y_2O_3, corresponding to different substrates and annealing temperature are shown in same figures (insets). The decay curves are fitted by single exponential function in a form: $I = I_0 \exp(-t/\tau)$, (τ is the 1/e lifetime of the rare earth ion). The lifetimes values of the Y_2O_3 doped Eu^{3+} thin films are presented in Table 2. We observe from the Table 2 that for Si (100) and Si (111) substrates, the decay time decreases between 500°C and 800°C despite the increasing the grain size and increase between 800°C and

950°C. For the corning substrate, the values of the lifetime increase from 500°C to 650°C. It is known that, the radiative lifetime of electric dipole transitions of an ion inserted in a medium could be expressed by [20]:

$$\tau_R \approx \frac{1}{f(ED)} \frac{\lambda_0^2}{[1/(3n^2+2)]^2 n}, \quad (1)$$

where $f(ED)$ is the oscillator strength for the electric dipole transition, λ_0 is the wavelength in vacuum, and n is the refractive index of the medium. It is know also that nanocrystallites occupy only a small fraction of the total volume, then, it is necessary to introduce an effective index of refraction for the medium, n_{eff}, which consists of the nanoparticles surrounded by the media with refractive index n_{med}. One may evaluate an effective index of refraction [20].

$$n_{eff}(x) = x n_{bulk} + (1-x) n_{med}, \quad (2)$$

where x is the "filling factor" showing which fraction of space is occupied by the nanocrystallites. For nanocrystallites n in Equation (3), is consequently replaced by $n_{eff}(x)$ (Equation (4)). The use of n_{eff} is valid when the average size of the particles is much smaller than the wavelength of light, which is true in this study. For $Y_2O_3 : Eu^{3+}$ bulk material, $n(Y_2O_3) = 1.91$ [21]. $Y_2O_3 : Eu^{3+}$ nanophosphor thin films are putted in the opposite side of air medium ($n_{air} = 1$) and the other side of the thin films is opposite to the substrate.

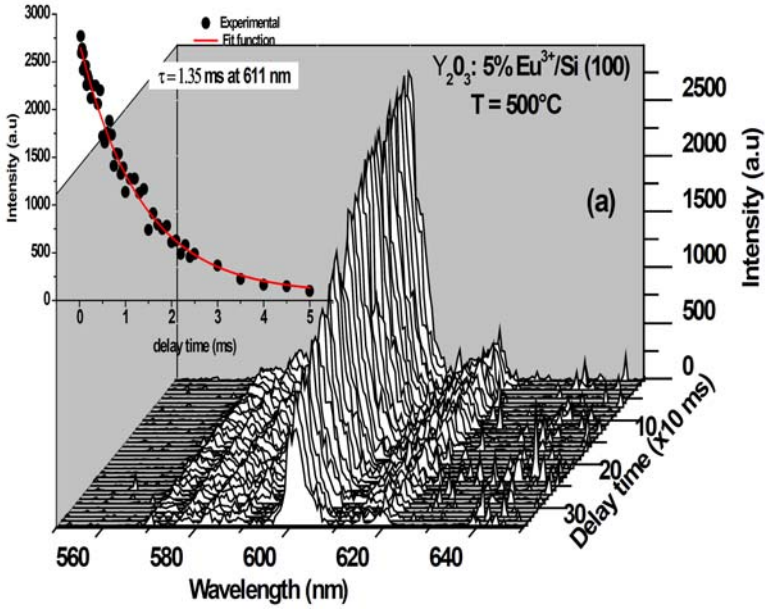
Experimental
Fit function
τ = 1.35 ms at 611 nm
Y2O3: 5% Eu3+/Si (100)
T = 500°C
(a)
Intensity (a.u)
delay time (ms)
Wavelength (nm)
Delay time (x10 ms)

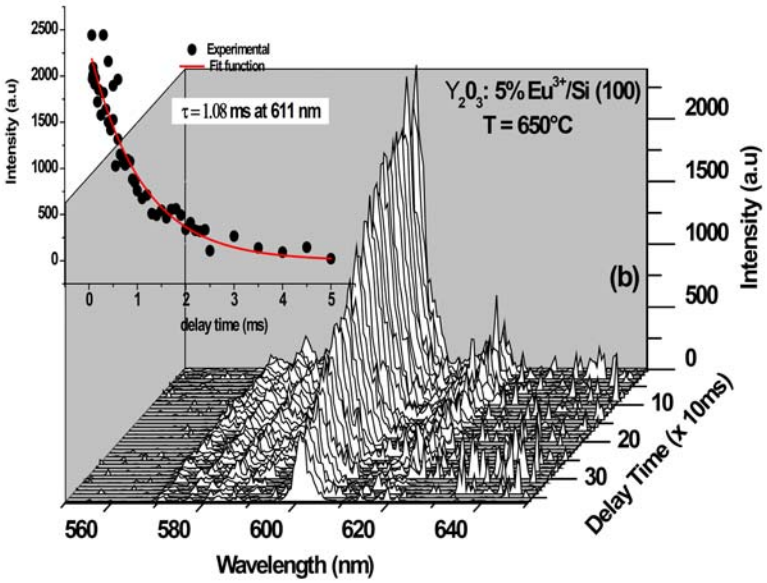
Experimental
Fit function
τ = 1.08 ms at 611 nm
Y2O3: 5% Eu3+/Si (100)
T = 650°C
(b)
Intensity (a.u)
delay time (ms)
Wavelength (nm)
Delay Time (x 10ms)

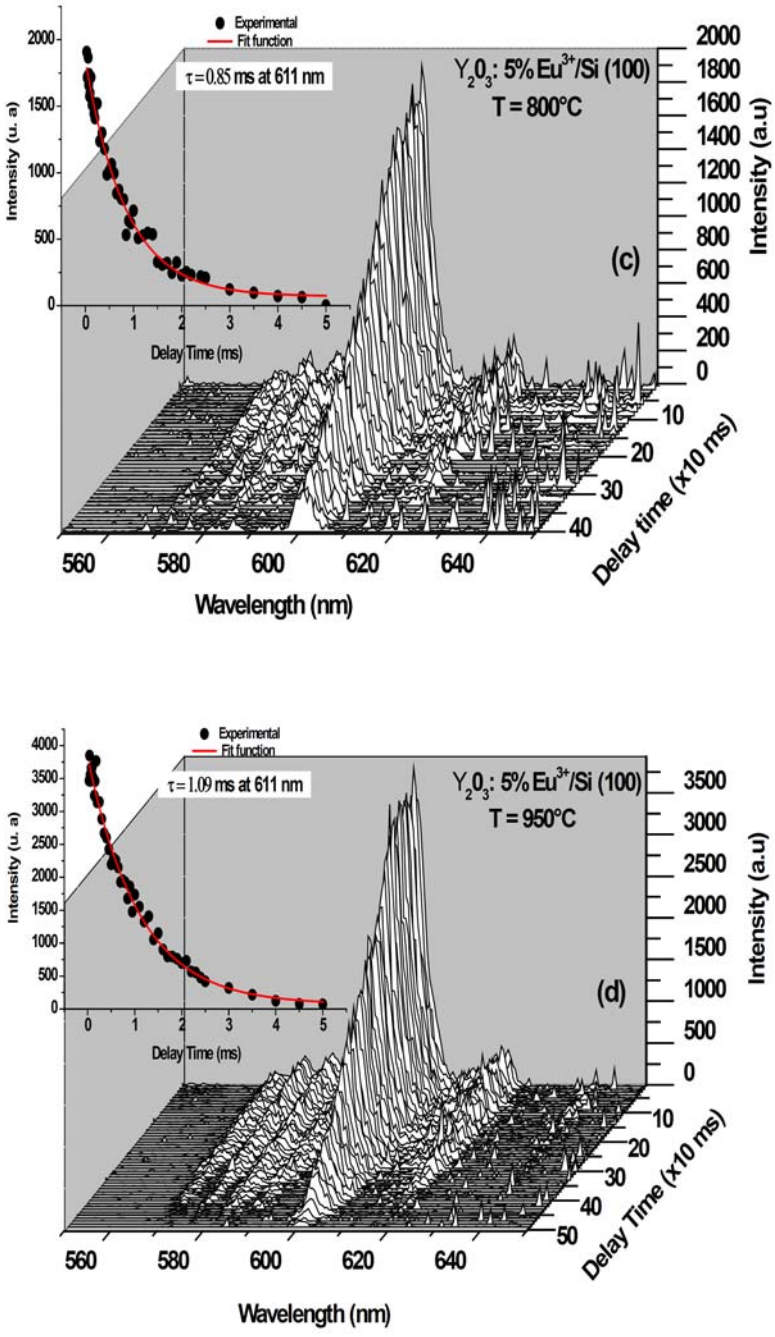
Experimental
Fit function
τ=0.85 ms at 611 nm
Y2O3: 5% Eu3+/Si (100)
T = 800°C
(c)
Intensity (u. a)
Delay Time (ms)
Intensity (a.u)
Delay time (x10 ms)
Wavelength (nm)
τ=1.09 ms at 611 nm
Y2O3: 5% Eu3+/Si (100)
T = 950°C
(d)
Delay Time (x10 ms)

Figure 8(a)

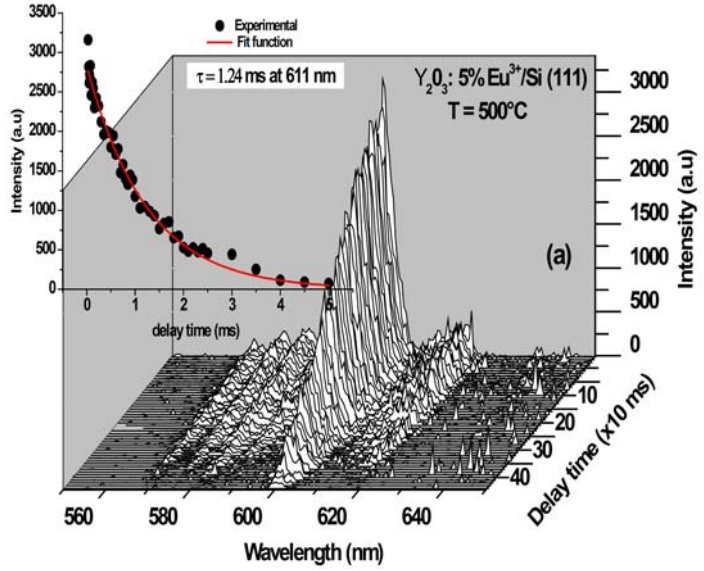
Experimental
Fit function
τ = 1.24 ms at 611 nm
Y2O3: 5% Eu3+/Si (111)
T = 500°C
(a)
Intensity (a.u)
delay time (ms)
Wavelength (nm)
Delay time (x10 ms)

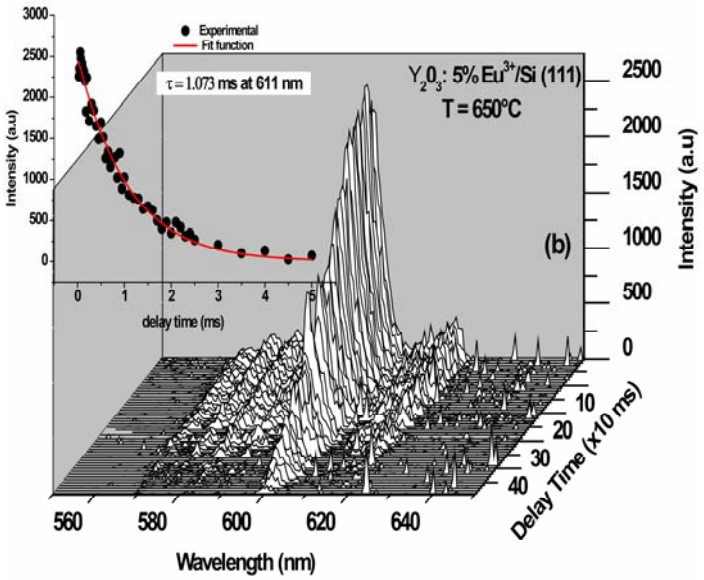
Experimental
Fit function
τ = 1.073 ms at 611 nm
Y2O3: 5% Eu3+/Si (111)
T = 650°C
(b)
Intensity (a.u)
delay time (ms)
Wavelength (nm)
Delay Time (x10 ms)

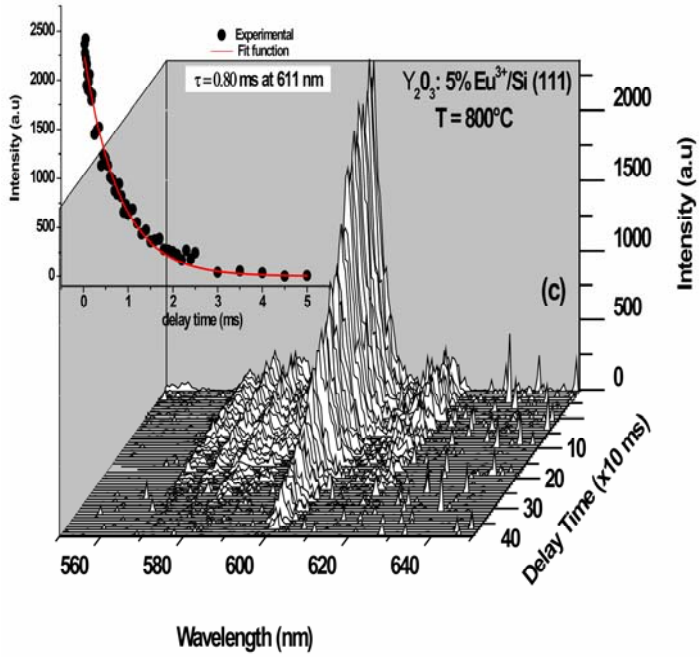
Experimental
Fit function
τ=0.80 ms at 611 nm
Y_2O_3: 5% Eu^{3+}/Si (111)
T = 800°C
(c)
Intensity (a.u)
delay time (ms)
Delay Time (x10 ms)
Wavelength (nm)

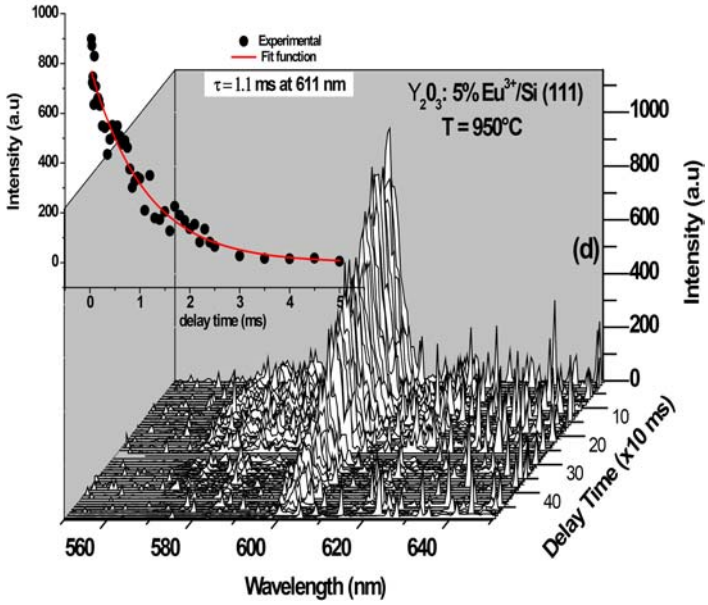
Experimental
Fit function
τ=1.1 ms at 611 nm
Y_2O_3: 5% Eu^{3+}/Si (111)
T = 950°C
(d)
Intensity (a.u)
delay time (ms)
Delay Time (x10 ms)
Wavelength (nm)

Figure 8(b)

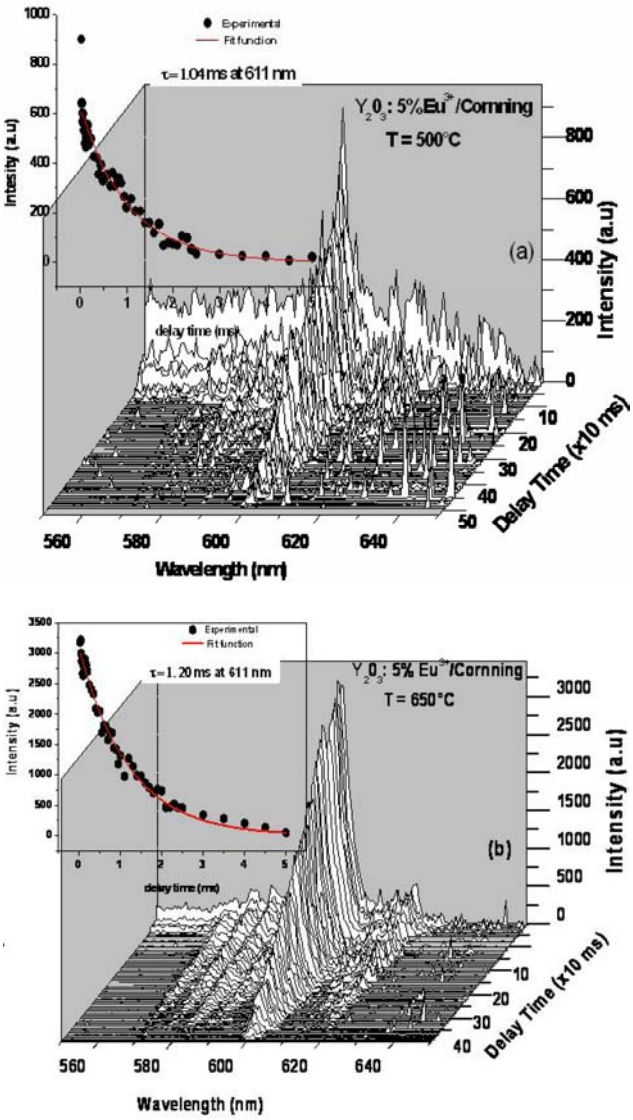

Figure 8(c)

Figure 8. 3D plots of room temperature emission spectra of Y_2O_3 : 5% Eu^{3+} thin films on Si (111), (a) 500ºC; (b) 650ºC; (c) 800ºC; (d) 950ºC upon UV excitation with variable time delay. Figures insets, normalized fluorescence decay curves for each temperature adjusted with single exponential decay.

Table 2. Refractive index and filling factor of $Y_2O_3 : 5\% Eu^{3+}$ on different substrate and at different annealing temperatures

	Si (100)				Si (111)				Corning glass	
	500	650	800	950	500	650	800	950	500	650
Lifetime (ms)										
n_{sample}	1.35	1.08	0.85	1.09	1.24	1.07	0.8	1.1	1.04	1.2
$x_{sample(in\ air\ medium)}$	1.69	1.80	1.90	1.80	1.74	1.81	1.89	1.80	1.83	1.75
	0.75	0.87	0.99	0.87	0.81	0.89	0.98	0.87	0.91	0.82

According to [21], from Equation (1), one can derive nonlinear equation which gives link between emission lifetimes of $^5D_0$ state in bulk and nanomaterial with effective index of refraction of sample:

$$\frac{\tau_{bulk}}{\tau_{sample}}(n_{bulk}^2 + 2)^2 n_{bulk} = n_{sample}^5 + 4n_{sample}^3 + 4n_{sample}, \quad (3)$$

and the optical filling factor is given by [21]:

$$x_{sample} = \frac{n_{sample} - n_{med}}{n_{bulk} - n_{med}}. \quad (4)$$

Knowing the value for the lifetime of bulk $Y_2O_3 : Eu^{3+}$, t_{bulk}, to be 0.9ms [19], we calculated refractive index (n_{sample}) and "optical filling factor" (x_{sample}) for each substrate and annealing temperature. As the luminescence is measured from the air side and if we assume that $Y_2O_3 : Eu^{3+}$ nanocrystallites are surrounded by the air, then $n_{med} = n_{air} = 1$ and $n(Y_2O_3) = 1.91$. The values of n_{eff} and x are determined and presented on Table 2. From Table 2, for Si (111) and Si (100) substrates and from 500ºC to 800ºC, the refractive index increases, this can be related to the increases of the crystallinity. While it decreases for 950ºC, despite the increases of it grain size. For corning glass, the refractive index decreases from 500ºC to 650ºC.

According to Lee et al. [22], the fraction of escaping light is approximately $1/4n^2$, where n is refractive index. Indeed, the extraction of the light from $Y_2O_3 : Eu^{3+}$ thin films nanophosphors with modulated refractive index are the key to explain these behaviours.

In Figure 9 ((a), (b) and (c)), we plot the variation of $^5D_0 \rightarrow {}^7F_2$ transition intensities and the fraction of escaping light $1/4n^2$ for different substrates and annealing temperatures. From the figure, we observe that they present the same behaviours, which can explain the former phenomenon. Indeed, the smaller is the value of refractive index, corresponding to the small grain size (low annealing temperature) of $Y_2O_3 : Eu^{3+}$ thin film, higher is the number of photons escaped from phosphor thin films. In addition, as seen from Table 2, it is important to note that for the same temperature and different substrate, n_{eff} presents a different values and consequently different x. This means that the other side which is the substrate, on which the films are deposed, has an effect, even if the emission go out from the side of air. We thought that it should take into account the effect of the substrate for x calculation. One can assume that $Y_2O_3 : Eu^{3+}$ nanocrystallites are embedded in unknown medium different from air $(n > 1)$ and the effective refractive index of this medium is calculated in such a way that x has a physical sense.

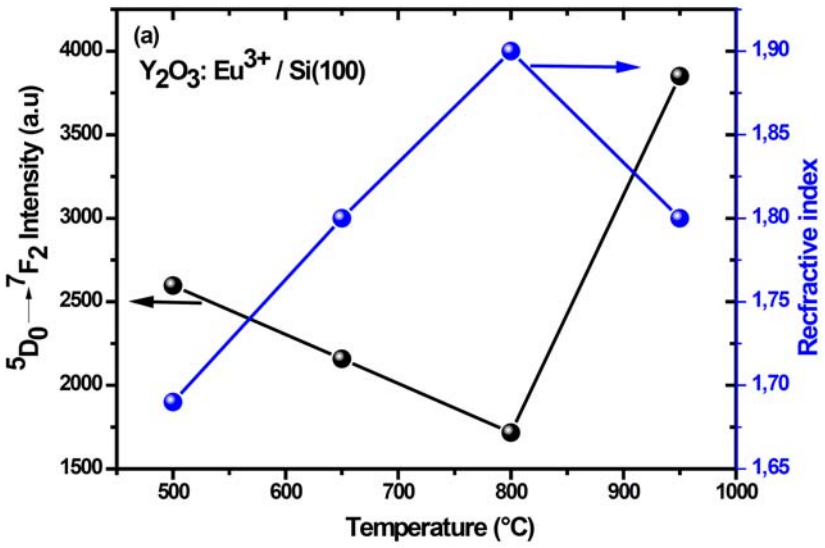
(a)
Y_2O_3: Eu^{3+} / Si(100)
$^5D_0 \rightarrow {}^7F_2$ Intensity (a.u)
Recfractive index
Temperature (°C)
4000
3500
3000
2500
2000
1500
1,90
1,85
1,80
1,75
1,70
1,65
500
600
700
800
900
1000

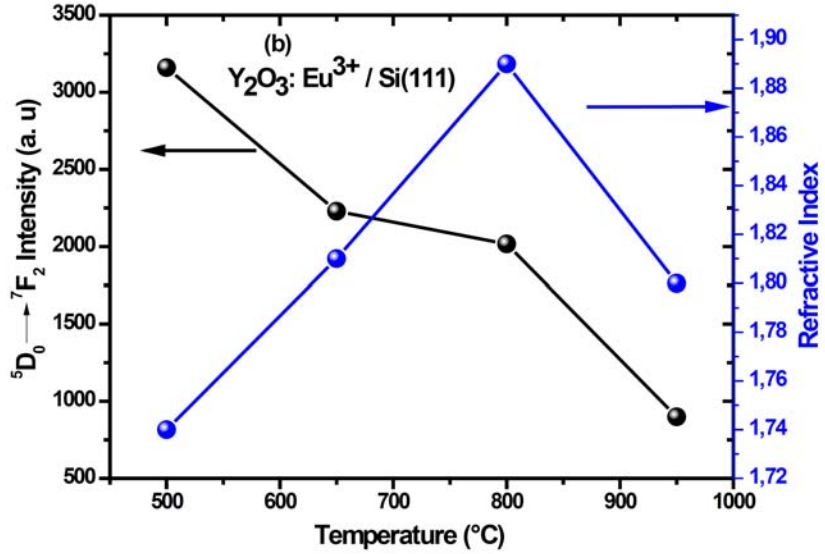
(b)
Y_2O_3: Eu^{3+} / Si(111)
$^5D_0 \rightarrow {}^7F_2$ Intensity (a. u)
Refractive Index
Temperature (°C)
3500
3000
2500
2000
1500
1000
500
1,90
1,88
1,86
1,84
1,82
1,80
1,78
1,76
1,74
1,72
500
600
700
800
900
1000

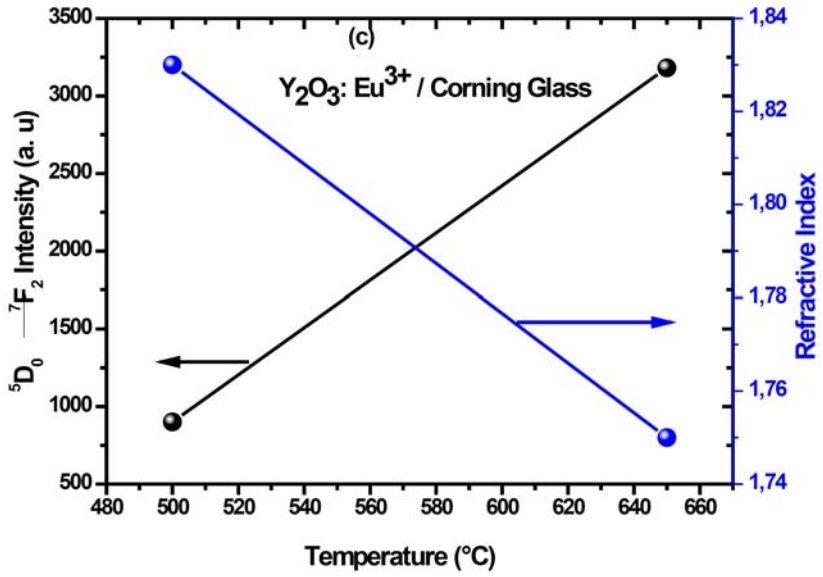

Figure 9. Variation of $^5D_0 \rightarrow ^7F_2$ transition intensities and the fraction of escaping light $1/4n^2$ for different substrates and annealing temperatures.

4. Conclusion

In summary, planar nano-crystalline Y_2O_3 : 5% Eu^{3+} nano-phosphor powders and thin films have been successfully grown on different substrates such as Si (100), Si (111), and corning glass, annealed at different temperatures, using sol-gel and spin-coating deposition techniques. The influences of substrate nature and annealing temperature, on structural, morphology and the steady and time resolve photoluminescence have been investigated. It is shown that, in all cases, Y_2O_3 exhibit a cubic phase of Y_2O_3 and it is found that the nanocrystallites sizes increase when increasing annealing temperature for Si (100), Si (111) substrates. Furthermore, crystalline and smooth Y_2O_3 : Eu^{3+} thin-film phosphors are obtained through the sol-gel spin

coating and annealing processes. Under UV (CTB band) excitation, the $Y_2O_3 : Eu^{3+}$ powders and films show intense red emission at the 611nm assigned to forced electric dipole transition $^5D_0 \rightarrow {}^7F_2$ of Eu^{3+} in C_2 cite. In addition, the time resolved photoluminescence and consequently, the lifetime shows a strong dependence on the nature and the annealing temperature influenced by the change of refractive index of $Y_2O_3 : Eu^{3+}$ thin films nanomaterial. In addition, it is found that the smaller is the value of refractive index $Y_2O_3 : Eu^{3+}$ thin film, higher is the number of photons escaped from phosphor thin films.

References

[1] F. W. Liu, C. H. Hsu, F. S. Chen and C. H. Lu, Ceramics International 38 (2012), 1577.

[2] J. S. Bae, J. H. Jeong, K. S. Shim, S. B. Kim, B. K. Moon and S. S. Yi, Thin Solid Films 476 (2005), 35.

[3] C. R. Ronda and B. M. J. Smets, Journal of the Electrochemical Society 136 (1989), 570.

[4] G. Wakefield, E. Holland and P. J. Dobson, Advanced Materials 13 (2001), 1557.

[5] G. Alarcon-Flores, M. García-Hipolito, M. Aguilar-Frutis, S. Carmona-Tellez, R. Martinez-Martinez, M. P. Campos-Arias, E. Zaleta-Alejandre and C. Falcony, Materials Chemistry and Physics 149-150 (2015), 34.

[6] L. Loua, W. Zhang, A. Brioude, C. Le Luyer and J. Mugnier, Optical Materials 18 (2001), 331.

[7] L. Wang, L. Shi, N. Liao, H. Jia, X. Yu, P. Du, Z. Xi and D. Jin, Thin Solid Films 518 (2010), 4817.

[8] S. L. Jones, D. Kumar, F. K. Singh and P. H. Holloway, Applied Physics Letters 71 (1997), 404.

[9] W. M. Li, M. Ritala, M. Leskela, L. Niinisto, E. Soininen, S. S. Sun, W. S. Tong and C. J. Summers, Journal of Applied Physics 86 (1996), 439.

[10] T. Minami, Y. Kuroi and S. Takata, Journal of Vacuum Science & Technology A 14 (1996), 1736.

[11] G. A. Hirata, J. McKittrick, M. Avalos-Borja, J. M. Siqueiros and D. Devlin, Applied Surface Science 113(114) (1997), 509.

[12] J. A. Ruffner, R. T. Tuenge, S. S. Sun, P. D. Grandon and P. F. Hlava, Thin Solid Films 310 (1997), 123.

[13] W. G. Shin, M. Park, J. Kim, S. W. Joo, I. Cho and Y. Sohn, Thin Solid Films 565 (2014), 293.

[14] L. S. Wang, Y. H. Zhou, Z. W. Quan and J. Lin, Materials Letters 59 (2006), 1130.

[15] J. Y. Cho, K-Y. Ko and Y. R. Do, Thin Solid Films 515 (2007), 3373.

[16] L. Guerbous, M. Seraiche and O. Krachni, Journal of Luminescence 134 (2013), 165.

[17] A. Boukerika and L. Guerbous, Journal of Luminescence 145 (2014), 148.

[18] L. Guerbous and A. Boukerika, Journal of Nanomaterials, Volume 2015, ID 617130.

[19] L. Lamiri, L. Guerbous, M. Samah, A. Boukerika and S. Ouhenia, Luminescence 30 (2015), 1336.

[20] R. S. Meltzer, S. P. Feofilov, B. Tissue and H. B. Yuan, Physical Review B: Condensed Matter 60 (1999), R 14012.

[21] M. R. Krsmanovic, Z. Antić, M. G. Nikolić, M. Mitrić and M. D. Dramicanin, Ceramics International 37 (2011), 525-531.

[22] K. Lee, K.-Y. Ko and J. Ahn, Thin Solid Films 547 (2013), 222.

■